



Contents lists available at ScienceDirect

Nuclear Inst. and Methods in Physics Research, A

journal homepage: www.elsevier.com/locate/nima

Full Length Article



A compact start time counter using plastic scintillators readout with MPPC arrays for the WASA-FRS HypHI experiment

E. Liu^{1,2,3,*}, V. Drozd^{4,5}, H. Ekawa², S. Escrig⁶, Y. Gao^{1,2,3}, Y. He^{2,7}, A. Kasagi^{2,8,9}, M. Nakagawa², H. Ong^{1,10,11}, C. Rappold⁶, R. Sekiya^{12,13}, T.R. Saito^{2,5,7}, X. Tang¹, Y.K. Tanaka², H. Wang², A. Yanai^{2,14}, P. Achenbach^{15,16}, H. Alibrahim Alfaki⁵, F. Amjad⁵, M. Armstrong^{5,17}, K.-H. Behr⁵, J. Benlliure¹⁸, Z. Brencic^{19,20}, T. Dickel^{5,21}, S. Dubey⁵, M. Feijoo-Fontán¹⁸, H. Fujioka²², H. Geissel^{5,21}, F. Goldenbaum²³, A. Graña González¹⁸, E. Haettner⁵, M.N. Harakeh⁴, H. Heggen⁵, C. Hornung⁵, N. Hubbard^{5,24}, K. Itahashi^{12,25}, M. Iwasaki^{12,25}, N. Kalantar-Nayestanaki⁴, M. Kavatsyuk⁴, E. Kazantseva⁵, A. Khreptak^{26,27}, B. Kindler⁵, R. Knoebel⁵, H. Kollmus⁵, D. Kostyleva⁵, S. Kraft-Bermuth²⁸, N. Kurz⁵, B. Lommel⁵, S. Minami⁵, D.J. Morrissey²⁹, P. Moskal^{27,30}, I. Mukha⁵, A. Muneem^{2,31}, K. Nakazawa⁸, C. Nociforo⁵, S. Pietri⁵, J. Pochodzalla^{15,16}, S. Purushothaman⁵, E. Rocco⁵, J.L. Rodríguez-Sánchez^{18,32}, P. Roy⁵, R. Ruber³³, S. Schadmand⁵, C. Scheidenberger^{5,21}, P. Schwarz⁵, V. Serdyuk²³, M. Skurzok^{27,30}, B. Streicher⁵, K. Suzuki^{5,34}, B. Szczepanczyk⁵, N. Tortorelli⁵, M. Vencelj¹⁹, T. Weber⁵, H. Weick⁵, M. Will⁵, K. Wimmer⁵, A. Yamamoto³⁵, J. Yoshida^{2,36}, J. Zhao^{5,37}

¹ Institute of Modern Physics, Chinese Academy of Sciences, 730000 Lanzhou, China

² High Energy Nuclear Physics Laboratory, RIKEN Cluster for Pioneering Research, RIKEN, 351-0198 Wako, Saitama, Japan

³ School of Nuclear Science and Technology, University of Chinese Academy of Sciences, 100049 Beijing, China

⁴ University of Groningen, 9747 AA Groningen, The Netherlands

⁵ GSI Helmholtzzentrum für Schwerionenforschung GmbH, 64291 Darmstadt, Germany

⁶ Instituto de Estructura de la Materia - CSIC, 28006 Madrid, Spain

⁷ School of Nuclear Science and Technology, Lanzhou University, 730000 Lanzhou, China

⁸ Graduate School of Engineering, Gifu University, 501-1193 Gifu, Japan

⁹ Graduate School of Artificial Intelligence and Science, Rikkyo University, 171-8501 Tokyo, Japan

¹⁰ Joint Department for Nuclear Physics, Lanzhou University and Institute of Modern Physics, Chinese Academy of Sciences, 730000 Lanzhou, China

¹¹ Research Center for Nuclear Physics, Osaka University, 567-0047 Osaka, Japan

¹² Meson Science Laboratory, Cluster for Pioneering Research, RIKEN, 2-1 Hirosawa, 351-0198 Wako, Saitama, Japan

¹³ Kyoto University, 606-8502 Kyoto, Japan

¹⁴ Saitama University, Sakura-ku, 338-8570 Saitama, Japan

¹⁵ Institute for Nuclear Physics, Johannes Gutenberg University, 55099 Mainz, Germany

¹⁶ Helmholtz Institute Mainz, Johannes Gutenberg University, 55099 Mainz, Germany

¹⁷ Institut für Kernphysik, Universität Köln, 50923 Köln, Germany

¹⁸ IGFAE, Universidade de Santiago de Compostela, 15782 Santiago de Compostela, Spain

¹⁹ Jožef Stefan Institute, 1000 Ljubljana, Slovenia

²⁰ University of Ljubljana, 1000 Ljubljana, Slovenia

²¹ Universität Gießen, 35392 Gießen, Germany

²² Tokyo Institute of Technology, 152-8550 Tokyo, Japan

²³ Institut für Kernphysik, Forschungszentrum Jülich, 52425 Jülich, Germany

²⁴ Institut für Kernphysik, Technische Universität Darmstadt, 64289 Darmstadt, Germany

²⁵ Nishina Center for Accelerator-Based Science, RIKEN, 2-1 Hirosawa, 351-0198 Wako, Saitama, Japan

²⁶ INFN, Laboratori Nazionali di Frascati, Frascati, 00044 Roma, Italy

²⁷ Institute of Physics, Jagiellonian University, 30-348 Kraków, Poland

²⁸ TH Mittelhessen University of Applied Sciences, 35390 Gießen, Germany

²⁹ National Superconducting Cyclotron Laboratory, Michigan State University, MI 48824 East Lansing, USA

³⁰ Center for Theranostics, Jagiellonian University, 30-348 Kraków, Poland

* Corresponding author at: Institute of Modern Physics, Chinese Academy of Sciences, 730000 Lanzhou, China.

E-mail address: liueq@impcas.ac.cn (E. Liu).

<https://doi.org/10.1016/j.nima.2024.169384>

Received 5 September 2023; Received in revised form 26 March 2024; Accepted 17 April 2024

Available online 29 April 2024

0168-9002/© 2024 Published by Elsevier B.V.

³¹ Faculty of Engineering Sciences, Ghulam Ishaq Khan Institute of Engineering Sciences and Technology, 23640 Topi, Pakistan

³² CITENI, Campus Industrial de Ferrol, Universidade da Coruña, E-15403 Ferrol, Spain

³³ Uppsala University, 75220 Uppsala, Sweden

³⁴ Ruhr-Universität Bochum, Institut für Experimentalphysik I, 44780 Bochum, Germany

³⁵ KEK, 305-0801 Tsukuba, Ibaraki, Japan

³⁶ Tohoku University, 980-8578 Sendai, Japan

³⁷ Peking University, 100871 Beijing, China

ARTICLE INFO

Keywords:

Start time counter

Time resolution

MPPC array

ABSTRACT

We have developed a compact detector for measuring beam particles using plastic scintillators readout through Multi-Pixel Photon Counters, which is employed for hypernuclear measurements in the WASA-FRS experiment at GSI. The Time-of-Flight resolution of the newly-developed detector has been investigated in relation to the overvoltage with respect to the breakdown voltage, a maximum counting rate of approximately 3×10^6 /s per segment, and a maximum beam charge of $Z = 6$. The evaluated Time-of-Flight resolutions between the neighboring segments of the detector range from 44.6 ± 1.3 ps to 100.3 ± 3.6 ps (σ) depending on the segment, overvoltage values, and beam intensity. It is also observed that the Time-of-Flight resolution is inversely correlated to the beam atomic charge (Z).

1. Introduction

Experimental studies on hypernuclei, which are sub-atomic bound systems containing at least one hyperon, contribute to understand the strong interaction under the flavored-SU(3) symmetry [1,2]. Hypertriton, the simplest and lightest hypernucleus consisting of a proton, a neutron and a Λ hyperon, is considered as a benchmark in hypernuclear physics. However, its lifetime still remains as a puzzle, as briefly summarized in Ref. [3]. To precisely determine the hypertriton lifetime, the WASA-FRS HypHI experiment [3–7] has been performed in 2022 with the Fragment Separator (FRS) [8] at the GSI facility using the central detectors of the Wide Angle Shower Apparatus (WASA) [9]. The WASA central detectors and their associated detectors, including a start time counter and seven fiber tracker stations are placed in the mid-focal plane of the FRS, indicated as F2 in Fig. 1. Fig. 2 shows a schematic drawing of the detectors at F2. The details of the setup are described in Section 3.1.

Light hypernuclei, including hypertritons, are produced via projectile fragmentation reactions of relativistic ${}^6\text{Li}$ beams at 1.96 AGeV bombarding on a ${}^{12}\text{C}$ target, and it is aimed to observe the two-body mesonic decay of hypertritons, (${}^3_\Lambda\text{H} \rightarrow {}^3\text{He} + \pi^-$). The π^- mesons from hypertriton decays are measured using the WASA central detectors and associated detectors, while the decay residues, that is, ${}^3\text{He}$, are measured by the FRS. Meanwhile, various charged particles from the projectile fragment reactions, including π^- , π^+ , K^+ and protons, are also measured by the WASA central and associated detectors.

To reconstruct the invariant mass of the hypertriton events, the identification of charged particles measured by the WASA central detectors is required. Fig. 3 shows the particle identification plots with the WASA central and associated detectors located in the FRS F2 based on data produced using Monte Carlo simulations. A correlation between the velocity (β) and momentum divided by charge of particles is used for the identification. The momentum and the sign of the charge of particles are determined based on their tracks in the magnetic field using the GENFIT tracking package [10]. The velocity of particle is deduced from the measured track length and Time-of-Flight (TOF) between the start time counter (Timing-Zero counter, referred as a T0 counter in Figs. 1 and 2) and a plastic scintillator barrel (denoted as PSB in Fig. 2) [11]. Figs. 3(a) and 3(b) show the particle identification plot and the corresponding mass distribution, respectively, assuming a TOF resolution of approximately 110 ps, i.e., a time resolution of 80 ps for the T0 counter, which is similar to that of the PSB [11]. A clear separation between the different particles is observed. Similar plots were also produced for comparison by assuming a TOF resolution of 200 ps, as shown in Figs. 3(c) and 3(d). Consequently, a clearer

separation between identified particles was observed with a better TOF resolution. In this study, the following were required to develop the T0 counter:

1. It is desirable for the T0 counter to achieve a time resolution (σ) of less than 80 ps, which is similar to that of the PSB [11]. Therefore, a TOF resolution better than approximately 110 ps should be achieved to ensure a reasonable particle identification.
2. Because the total beam intensity is expected to be approximately 20 MHz with a horizontal beam spot size of $\sigma = 6$ mm in the Gaussian distribution, a stable performance of the T0 counter under high intensity heavy-ion beam is also required.
3. The T0 counter was originally designed to be installed right in front of the target, where the space is limited by the two fiber tracker stations, UFT1 and UFT2. Therefore, the T0 counter should have a compact size that allows assembly alongside the WASA central and their associated detectors.

The new T0 counter was developed fulfilling these requirements for the WASA-FRS HypHI experiment. The time resolution performance of the new T0 counter has been investigated using ${}^6\text{Li}$ beams at 1.96 AGeV with an maximum intensity of approximately 20 MHz. The beam atomic charge (Z) dependence of the time resolution has also been studied using a proton beam at 2.5 GeV and ${}^6\text{Li}$ and ${}^{12}\text{C}$ beams at 1.96 AGeV. In this paper, the evaluated time resolution performance of the newly-developed T0 counter is reported. The structure and configuration of the T0 counter are described in Section 2, and the configuration and setup for the WASA-FRS HypHI experiment are introduced in Section 3.1. Subsequently, Section 3.3 describes the analysis procedures, and the obtained results are discussed in Section 4.

2. Design of the T0 counter

The Multi-Pixel Photon Counter (MPPC) offers excellent time resolution under a large photon flux, and its compact size provides opportunities to make a small and fast detector by combining with small plastic scintillators. Moreover, it has become popular because of the lower cost, immunity to a magnetic field and lower operating voltage compared to photomultiplier tubes (PMTs). Therefore, MPPCs have been widely used in high energy and nuclear physics experiments for fast-timing measurements [11–18]. We have newly developed the T0 counter for the WASA-FRS HypHI experiment using MPPCs in combination with fast-timing plastic scintillators.

A schematic view of the T0 counter is shown in Fig. 4. It consists of 28 plastic scintillators with a size of $45 \text{ mm} \times 1.5 \text{ mm} \times 1.5 \text{ mm}$. We adopted the EJ-232 plastic scintillators from Eljen Technology with a refractive index of 1.58, a rise time of 0.35 ns and a decay time of 1.6 ns. Such a small segmentation design reduces the counting rates on

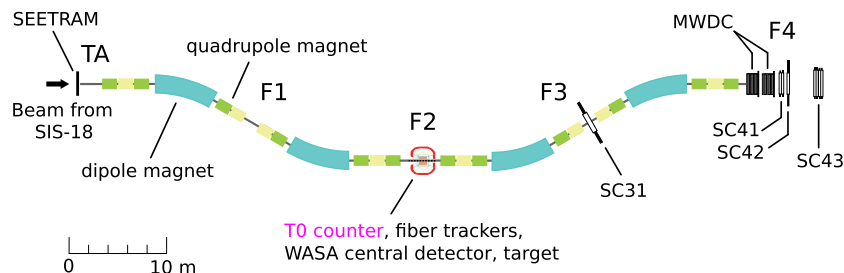


Fig. 1. A schematic overview of the FRS configuration during the WASA-FRS HypHI experiment. See the text for details.

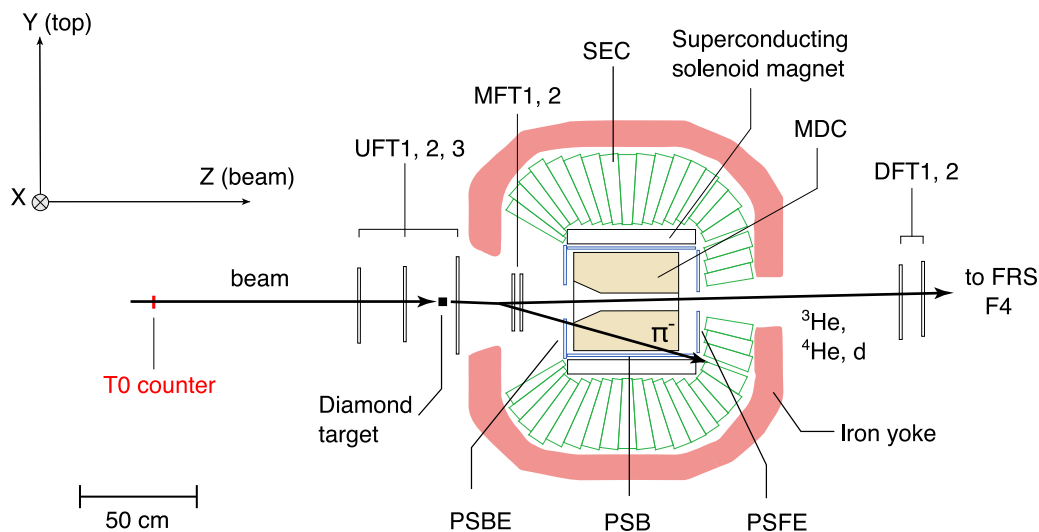


Fig. 2. A schematic view of the detailed setup at FRS-F2 used in the WASA-FRS HypHI experiment. See the text for details.

each segment, and thus, a stable performance can be achieved. Owing to the small size of the scintillators and limited space between them, it is impossible to directly collect photons from each scintillator using an individual MPPC. Additional light guides, for example made by fibers, were not adopted, because they will lead to a degradation of the time resolution [19]. Therefore, we came to the unique design using the MPPC array, Hamamatsu S13615-1025N-04 [20] coupling to four small plastic scintillator bars. Both sides of each scintillator segment are coupled to MPPCs using optical grease (TSK5353, Momentive Performance Materials) directly.

Each MPPC array consists of 4×4 channels, and each channel has as an effective photosensitive area of $1.0 \text{ mm} \times 1.0 \text{ mm}$ with a 0.2 mm pitch between the adjacent channels. Each channel has 1584 pixels with a pixel pitch of $25 \text{ }\mu\text{m}$. The total size of each MPPC array is $4.85 \text{ mm} \times 4.85 \text{ mm}$. The breakdown voltage in the specification is $\sim 53 \text{ V}$. The MPPCs are arranged on a PCB board, as shown in Fig. 5(a). Seven MPPCs arrays are placed into two rows in the Z direction. They are seamlessly aligned along the X direction, while the neighboring MPPCs are physically separated with different Z position. Bias voltage to the MPPC is applied using a Kikusui PMX350-0.2A power supply [21]. A schematic top view of the PCB board with the coupled scintillators is shown in Fig. 5(b), where the gray boxes labeled with numbers corresponding to the scintillators. Four scintillators are coupled to the centers of four selected channels of each MPPC array, as highlighted by the red boxes in Fig. 5(a). This arrangement physically separates adjacent scintillators while allowing for a $0.25\text{--}0.3 \text{ mm}$ overlap in the X direction, ensuring that beam particles will interact with at least one scintillator segment. The size of the scintillator with a cross section of $1.5 \text{ mm} \times 1.5 \text{ mm}$ can also guarantee the mechanical strength and can prevent deformation. The combined configuration of scintillators and MPPCs results in an effective detection area of approximately 34 mm

in the X direction and 45 mm in the Y direction, which matches the beam spot size.

3. Measurements and analysis

3.1. Experimental setup

Fig. 1 represents an overview of the configuration used in the WASA-FRS HypHI experiment. The T0 counter, the WASA central detector, additional detectors and a diamond target (^{12}C) are installed at the central focal plane of the FRS (F2). Beams extracted from the SIS-18 synchrotron bombard on the diamond target. Light hypernuclei produced in nuclear reactions can fly forward and decay in-flight behind the target since they were boosted. Light charged particles from the decay and beam reactions at the target are detected by the WASA central detectors and associated detectors, while particles emitted to the forward direction around at 0° are transported through the second half of the FRS (F2-F4) and are measured by plastic scintillators SC31 in F3, SC41, SC42 and SC43 in F4, as well as two multi-wire drift chambers (MWDCs) at F4.

The detailed setup at F2 is illustrated in Fig. 2. The T0 counter is placed at the entrance of FRS-F2 in front of the other all detectors to measure beams particles, and it defines the start timing of the TOF measurements. The WASA central detector consists of a mini-drift chamber (MDC), a plastic scintillator barrel (PSB), a forward end-cap (PSFE), a backward end-cap (PSBE), a superconducting solenoid magnet [22,23] as well as a scintillator electromagnetic calorimeter (SEC). Additional fiber trackers (UFTs, MFTs and DFTs) are installed to measure trajectories of charged particles. They are used for determining primary and decay vertices, which are essential to deduce the lifetime of hypernuclei.

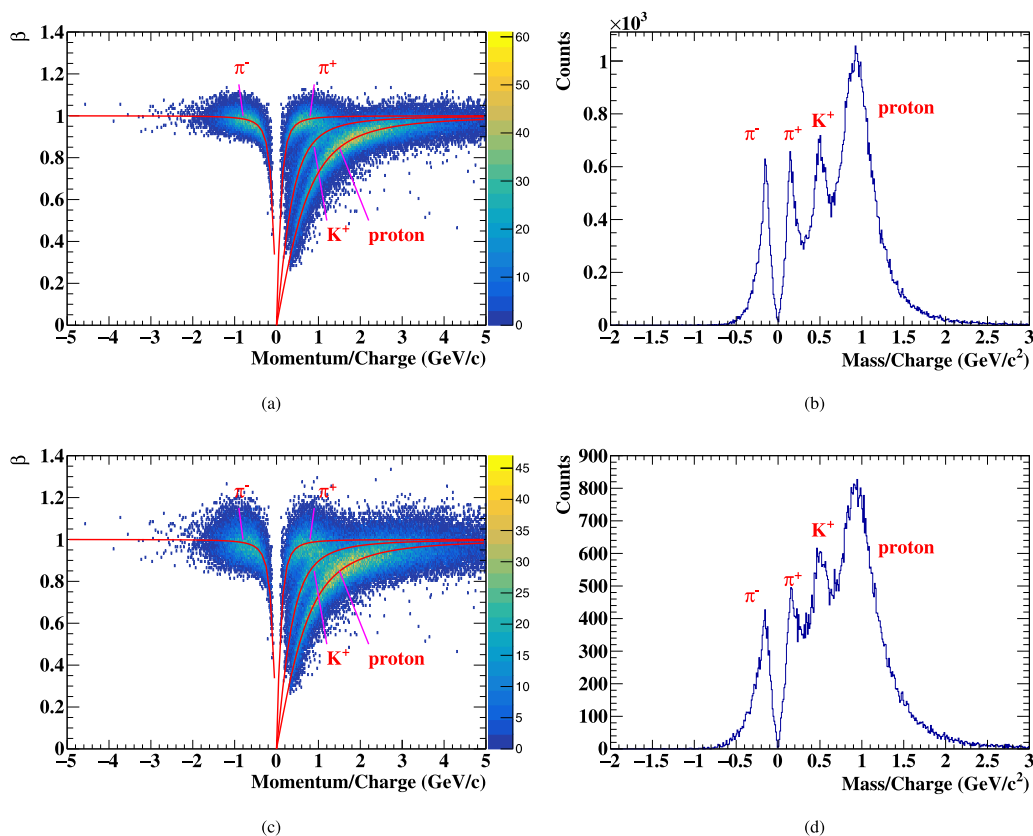


Fig. 3. Particle identification plots using the Monte Carlo simulation: (a) with a TOF resolution of approximately 110 ps, that is, a T0 counter time resolution of 80 ps, which is similar to that of the PSB. The abscissa shows the momentum divided by the charge, and the ordinate shows the velocity normalized to the speed of light (β). (b) The distribution of deduced masses from (a), the abscissa shows the mass divided by charge. (c) Same plot as (a), with an assumed TOF resolution of 200 ps, that is, a T0 counter time resolution of 183 ps. (d) The distribution of deduced masses from (b), the abscissa shows the mass divided by charge.

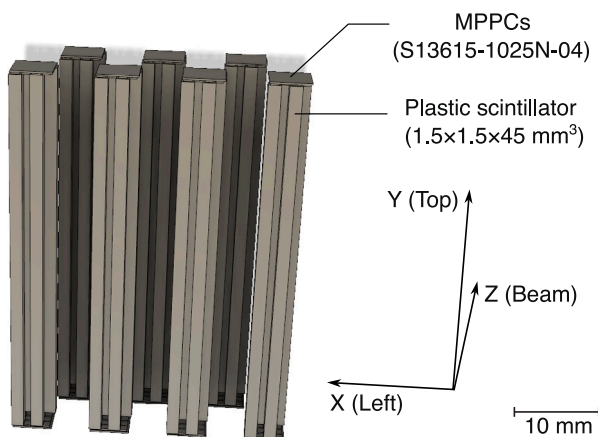


Fig. 4. The schematic view of the T0 counter. It consists of 28 plastic scintillators with a size of 45 mm \times 1.5 mm \times 1.5 mm. Every 4 adjacent segments are coupled to one MPPC. Both sides of each segment were readout.

The experiment was commissioned with proton beams at 2.5 GeV, and the hypernuclear production measurement was performed with ${}^6\text{Li}$ and ${}^{12}\text{C}$ beams at 1.96 AGeV. A total spill length of beam is approximately 12 s. To monitor the beam intensity during the experiment, counting rates of a secondary electron transmission monitor (SEETRAM) [24], SC41 and four selected segments (6, 14, 15 and 22) of the T0 counter are recorded by using a CAEN V830 module.

For the T0 counter, analogue signals from both sides of each segment are amplified by using the amplifiers that had been developed

Table 1

The parameters applied to the MCFD-16 modules for the T0 counter.

Parameter	Gain	Fraction	Delay
Value	3	20%	2 ns

in Ref. [18]. The analogue signals after amplification are converted to logic signals by using the Mesytec MCFD-16 modules [25]. Therefore, the dependence of the timing on the amplitude is removed. The CFD parameters used in the experiment are listed in Table 1. The hit timing information is then recorded by using CAEN V1290 Time-to-Digital Converter (TDC) modules. In addition, the charge information from each MPPC channel is also recorded by CAEN V792 Charge-to-Digital Converter (QDC) modules, which allows for the identification of beam particles. Analyses of recorded data are described in Section 3.3.

3.2. Intensity analysis

The ${}^6\text{Li}$ beam counting rate on the segment 14 is estimated to investigate the intensity dependence of the time resolution of the T0 counter for ${}^6\text{Li}$ beams, because the segment 14 is at the center of the beam spot and a higher intensity is measured at this point. We have recorded the counting rate on the segment 14 using a CAEN V830 scaler. However, owing to the effects of noise and δ rays, it was higher than the actual counting rate on it. Therefore, the actual counting rate of ${}^6\text{Li}$ on it is estimated using two steps. First, the total beam intensity delivered to FRS-F2 is estimated. Subsequently, the beam profile at the T0 counter position is estimated based on the measured track information using the two fiber tracker stations, UFT1 and UFT2. Consequently, it is estimated that $9.3\% \pm 0.1\%$ of the total beam intensity would hit the segment 14.

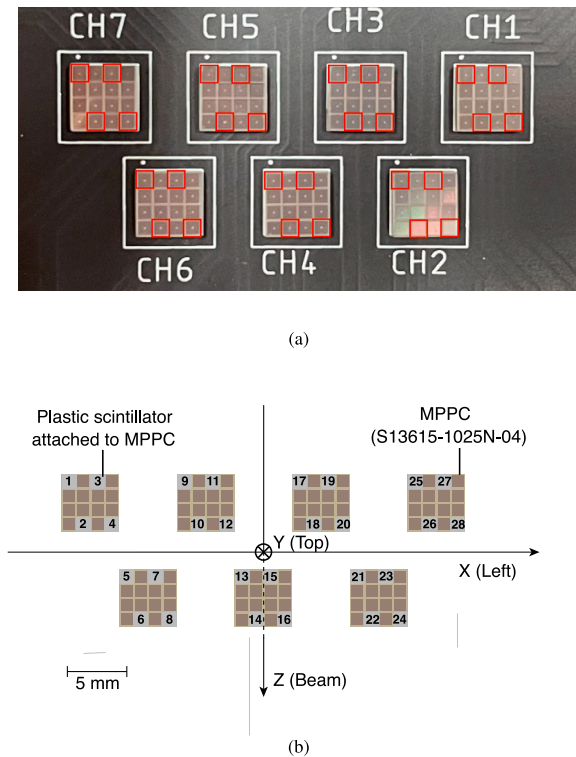


Fig. 5. (a) A photo of the PCB board for the MPPC array readout of the T0 counter. Four channels marked in red in each MPPC array are selected to read out the signals from the scintillators, as highlighted with the red boxes. All the other channels are not biased. (b) A schematic top view of the T0 counter installed in the experiment.

Therefore, the actual counting rate on the segment 14 is deduced by scaling the total beam intensity by 0.093.

The total beam intensity is analyzed using three different methods depending on the intensity range. Firstly, the total beam intensity is estimated using the SEETRAM detector, which was calibrated to the absolute ${}^6\text{Li}$ intensity. Secondly, the SC41 counting rate is used to measure the total beam intensity lower than 10 MHz, because the SEETRAM detector is only sensitive to ${}^6\text{Li}$ beams at 1.96 AGeV with an intensity larger than 10 MHz. While, the SC41 counting rate is much lower and sensitive to a lower total beam intensities, it maintains a linear correlation to the high total beam intensity owing to the limited FRS acceptance and low production rate of the ${}^3\text{He}$. Therefore, it can cover a wide range of the intensity measurement. A correlation between the SC41 counting rate and the total beam intensity measured using the SEETRAM detector is shown in Fig. 6. The correlation is fitted with a linear function, as shown by the red line in the plot. In this manner, the SC41 counting rate is calibrated to the total beam intensity, i.e., the total beam intensity could be estimated using the SC41 counting rate. Lastly, the scaler-recorded counting rate of the segment 14 is used to measure the total beam intensity when the counting rate on segment 14 is lower than 100 kHz, because the SC41 counting rate is lower than 10 per 10 ms in this case, and the total beam intensity estimated via SC41 has a large uncertainty. It is noticed that although it is higher than the actual counting rate, the scaler-recorded segment 14 counting rate is linear to the SC41 counting rate when the actual counting rate on the segment 14 is lower than 100 kHz. Therefore, the total beam intensity could be estimated using the scaler-recorded counting rate on the segment 14.

The counting rate is measured over a time interval of approximately 10 ms, and the time information is obtained from a 100 kHz clock that was recorded using the same CAEN V830 module. For each intensity point, if the estimated intensities in a period longer than 30 ms are

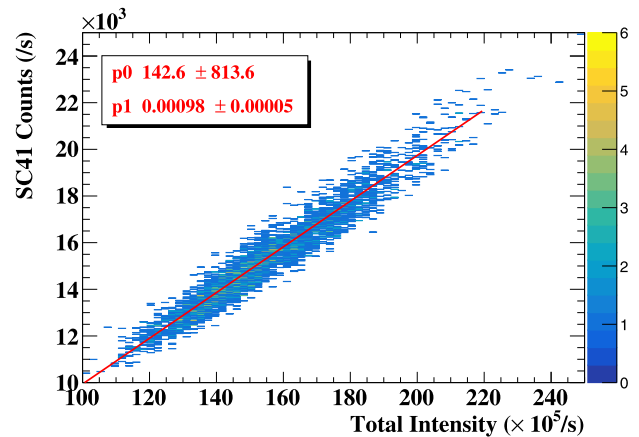


Fig. 6. Correlation between the total beam intensity and SC41 counting rate for a time interval of approximately 1 s. The total beam intensity is estimated using the SEETRAM detector, which is calibrated for the WASA-FRS HypHI experiment. The correlation is also fitted with a linear function, as denoted by the red line.

within $\pm 30\%$ of the selected intensity, the events during this period are used to estimate the time resolution of the T0 counter.

3.3. Estimation of the time resolution

Owing to the overlap of approximately 0.25 to 0.3 mm in the X direction between neighboring segments of the T0 counter, a certain portion of the beams can traverse through both segments. Therefore, the Time-of-Flight resolution between them can be estimated via the distribution, as shown in Fig. 8.

For segment i and its neighboring segment $i + 1$, the Time-of-Flight between them is calculated with

$$\text{TOF}_i = \frac{t_u^i + t_d^i}{2} - \frac{t_u^{i+1} + t_d^{i+1}}{2} \quad (1)$$

where t_u^i and t_d^i are the hit timings of the upper and bottom side of segment i in the Y direction, respectively. The TOF distribution is then fitted with a Gaussian function within a 3σ range, and the TOF resolution σ_{TOF}^i is then estimated using the standard deviation of the fitting result.

Fig. 7 represents a typical QDC spectrum for one side of the segment 14, which is positioned at the center of the beam spot, under a low-intensity ${}^6\text{Li}$ beam of $\sim\text{kHz}$. The events are selected when both sides of the segment 14 have TDC values in proper range. Therefore, the peak corresponding to pedestal is invisible in the plot. In addition to the prominent peak corresponding to ${}^6\text{Li}$ beam, a smaller peak on the left side is observed. This peak is caused by δ rays produced by beams interacting with the materials surrounding the T0 counter. It appears on the spectra for both sides of all the segments and leads to a degradation of the time resolution in the case with ${}^6\text{Li}$ beams. To exclude the δ ray events, the events with appropriate QDC values are selected, as indicated by the red shadowed region in Fig. 7. The TOF distribution for selected ${}^6\text{Li}$ beam events and δ ray events are shown in Fig. 8 in magenta and cyan lines, respectively. The ${}^6\text{Li}$ beam events refer to the events in which both the segment 14 and the segment 15 are hit by the ${}^6\text{Li}$ beams. The δ ray events are the events in which at least one of the segment 14 and the segment 15 is hit by δ rays. Both distributions are fitted by using a Gaussian function within a 3σ range and the fit results are shown in the same figure. It is observed that the TOF resolution is much better for selected ${}^6\text{Li}$ beam events with appropriate QDC values. Similar selections are applied for all the channels when investigating the overvoltage dependence and geometrical dependence of the TOF resolution.

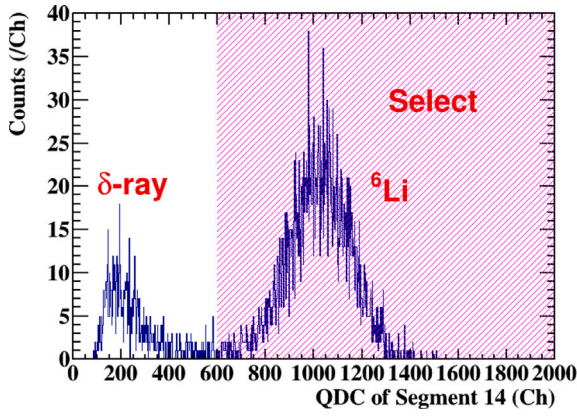


Fig. 7. A typical QDC distribution for the segment 14 of the T0 counter under low intensity ${}^6\text{Li}$ beam with an overvoltage of 2 V. The events are selected when both sides of the segment 14 have TDC values in proper range. Therefore, the peak corresponding to pedestal is invisible in the plot. Events with QDC value lies in the red shadowed region are selected for time resolution estimation.

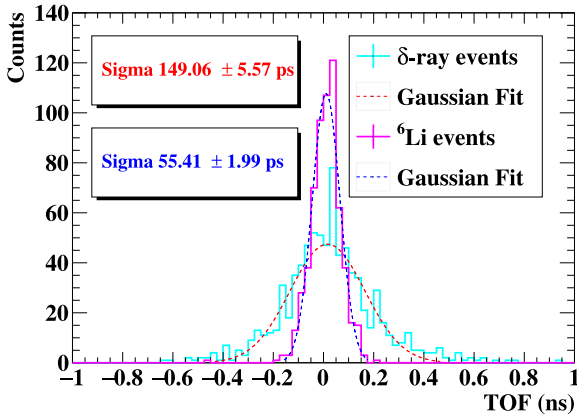


Fig. 8. Distribution of the TOF between the segment 14 and the segment 15. The histogram drawn with magenta lines is the distribution for selected events in which ${}^6\text{Li}$ beam particles hit both the segment 14 and the segment 15. The histogram drawn with cyan lines is the distribution for events in which at least one of the segments is hit by δ ray. Both distributions are fitted with a Gaussian function within a 3σ range. It is observed that the TOF resolution becomes better after selecting the ${}^6\text{Li}$ beam events.

In the case with proton beams, a single peak is observed in the QDC spectrum. It remains uncertain if δ ray events were included. When studying the beam charge dependence of the time resolution, proper selections with QDC values are implemented for ${}^6\text{Li}$ and ${}^{12}\text{C}$ beam data, while no selection is applied to the proton beam data. It is worth nothing that the TOF resolutions with proton beams may be affected by the δ rays.

As the beam intensity on each segment increases higher than approximately 19 kHz, the observed ${}^6\text{Li}$ beam peak in the QDC spectrum is gradually displaced towards the δ ray peak, caused by the gain degradation of the MPPCs [26–28]. Consequently, it becomes impossible to separate them via a QDC selection. The expected horizontal distribution of δ ray events is considered to be more flat and wider than that of beam particles, since the δ rays are scattered from the surrounding materials, while the horizontal beam spot size is ~ 6 mm (σ). Thank to the segmented design, the impacted T0 segment could provide a coarse X position of the particles including beam particles and δ -rays. Meanwhile, the tracks of the beam particles could be reconstructed and their X positions at the location of the T0 counter could be extrapolated from the hit positions of the UFT1 and UFT2. We selected events in which the absolute value of the residuals between the X positions obtained from these two different approaches is smaller than ~ 3 mm. In

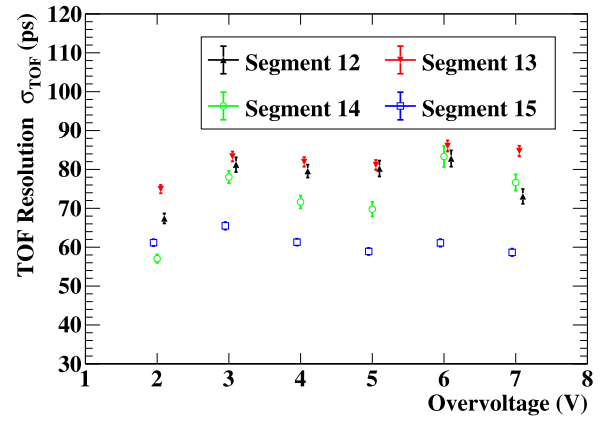


Fig. 9. The TOF resolutions of several neighboring segment combinations of the T0 counter under different overvoltages with respect to the breakdown voltage reported in the specification [20].

addition, the events in which the multiplicity of the T0 counter equals to two are selected to further exclude the δ ray events. For the analysis of the intensity dependence of the TOF resolutions, no QDC selection but the combination of these two selections are applied for the entire intensity range to ensure equal treatment for all of the data sets.

4. Results and discussion

The TOF resolutions between the neighboring segments of the T0 counter are estimated, and its dependence on the operation overvoltage, segment combinations, beam intensity, beam charge Z are presented.

4.1. Overvoltage dependence and segment dependence

The influence of the operation overvoltage on the TOF resolutions has been studied using ${}^6\text{Li}$ beams at 1.96 AGeV with a total beam intensity lower than 100 kHz. The overvoltage values with respect to the breakdown voltage reported in the specification [20] were varied from 2 V to 7 V at a step of 1 V. The results are shown in Fig. 9. The four segments that were read out using one MPPC array at the center of the beam profile are shown in the plot for representation, and the others have similar results. The observed differences between TOF resolutions with different operation overvoltage values are less than 26.3 ± 1.6 ps. Additionally, the dependence varies between different combinations of the neighboring segments.

The TOF resolutions for different neighboring segment combinations under varying operation overvoltage values are shown in Fig. 10. The results for 12 neighboring segment combinations at the center of the beam profile are shown. The others segments at the edge of the T0 counter are not shown owing to their low statistics, even though they have better TOF resolutions but with larger uncertainties. The TOF resolution also varies with different neighboring segment combinations, ranging from 44.6 ± 1.3 ps to 86.0 ± 1.4 ps, and the dependence is similar under different operation overvoltage values.

The TOF resolution is related to the time resolutions of both segments with

$$\sigma_{\text{TOF}}^i = \sqrt{\sigma_i^2 + \sigma_{i+1}^2} \quad (2)$$

where the σ_i and σ_{i+1} are the time resolutions of the segment i and $i+1$, respectively, which can be estimated with $\sigma_{\text{TOF}}^i = \sqrt{2}\sigma_i$, if $\sigma_i = \sigma_{i+1}$. Therefore, the time resolution of each segment can be evaluated as $\sigma_i = \sigma_{\text{TOF}}^i / \sqrt{2}$. However, the segment combination dependence of the TOF resolutions indicates that the assumption $\sigma_i = \sigma_{i+1}$ does not hold. Therefore, the time resolution of individual segments is not evaluated

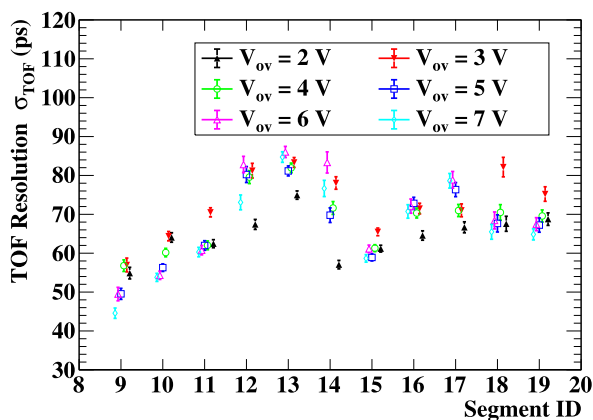


Fig. 10. TOF resolutions of different neighboring segment combinations of the T0 counter under different overvoltages V_{ov} with respect to the breakdown voltage reported in the specification [20]. It should be noted that not all neighboring segment combinations are listed in the plot because the segments at the edge of the T0 have small statistics owing to the beam profile.

using this method. Nevertheless, the presence of TOF resolutions better than 86.0 ± 1.4 ps indicates time resolution could be better than 80 ps.

Owing to the structure of the T0 Counter, some beam particles cross only one segment, while others cross two segments, and therefore have different energy loss. However, considering a flight length of approximately 1.3 m, the Time-of-Flight difference caused by this effect is smaller than 1 ps for 1.96 GeV/u ${}^6\text{Li}$ beam particles. Therefore, it is negligible since it is smaller than the measured TOF resolutions.

4.2. Intensity dependence

Fig. 11 represents the TOF resolution between segment 14 and 15 as a function of the counting rate on segment 14. The T0 counter is irradiated with ${}^6\text{Li}$ beams and the bias voltage applied to the T0 counter is 55 V. The observed TOF resolution gradually deteriorates as the beam intensity increases. This tendency in the dependence is consistent with the observation in Ref. [11]. Notably, segment 14 occupies the central position of the beam spot during the WASA-FRS HypHI experiment and consequently experiences the highest beam intensity among the T0 counter segments. Additionally, the maximum beam intensity observed in segment 14 reaches approximately 3 MHz, and the corresponding TOF resolution remains better than 100.3 ± 3.6 ps even though it is affected owing to the δ -rays. Considering the excellent time resolution of the PSB, this performance meets the requirement for the WASA-FRS HypHI experiment.

4.3. Beam charge dependence

The TOF resolutions of different neighboring segment combinations are investigated considering the beam charge Z and an overvoltage of 2 V using proton beams, ${}^6\text{Li}$ and ${}^{12}\text{C}$. The results for four segment combinations are shown in Fig. 12 as a representation, and the other combinations have a similar dependence. It is observed that the estimated TOF resolution of the T0 counter is inversely related to the beam charge Z . The TOF resolution in the case of ${}^6\text{Li}$ beams is drastically better than that in the case of proton beams, but similar to that in ${}^{12}\text{C}$ beam case. It has been reported in Refs. [11,18] that the time resolution is inversely proportional to the squared root of the energy loss $\sqrt{\Delta E}$ in the plastic scintillator. Since $\sqrt{\Delta E}$ is approximately proportional to the beam charge Z , the time resolution is expected to be inversely related to the beam charge Z for the minimum ionization particles. However, as we have discussed in Section 3.3, it remains uncertain if the δ rays are included or not in the case of proton beams, resulting

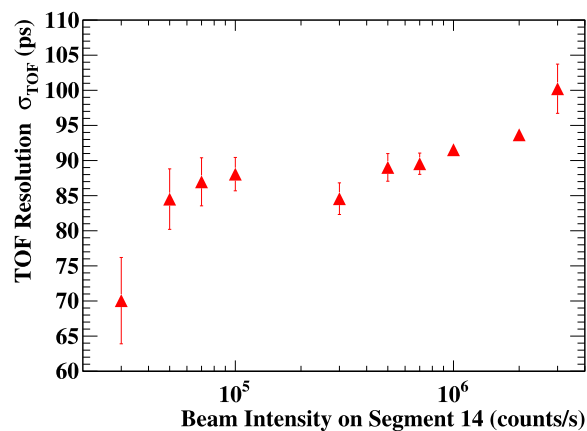


Fig. 11. Counting rate dependence of the TOF resolution between segment 14 and 15 under a ${}^6\text{Li}$ beam with an overvoltage of 2 V. The dependence worsens for intensities larger than 1 MHz.

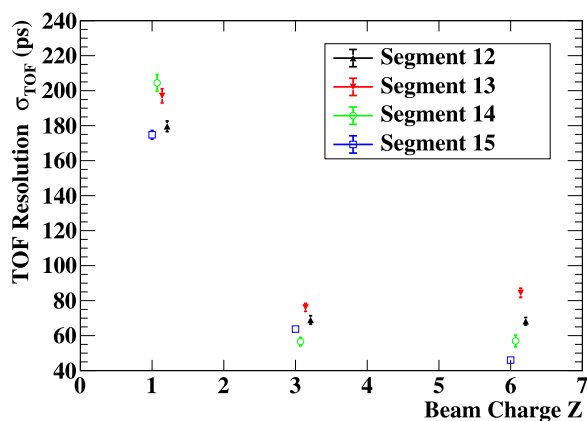


Fig. 12. Beam charge Z dependence on the TOF resolution under an overvoltage of 2 V and a low intensity beam. The dependence for the different segments are similar.

in some deviation from the estimated TOF resolution. Therefore, The tendency of the observed dependence is similar to the results reported in Refs. [11,18].

5. Summary

A compact and uniquely-designed start time counter for the hypernuclear measurements in the WASA-FRS HypHI experiment was developed in this study using plastic scintillators and MPPC arrays. The TOF resolutions between the neighboring segments of the T0 counter have been investigated with respect to different operation overvoltage, counting rates and beam atomic charges. The results show that the observed TOF resolutions of different neighboring segment combinations of the T0 counter are better than 86.0 ± 1.4 ps under ${}^6\text{Li}$ beams with a beam intensity lower than 100 kHz. The estimated TOF resolutions of different segment combinations vary with a difference of less than 41.4 ± 1.9 ps. Additionally, the dependence under an applied overvoltage range from 2 V to 7 V is similar, and the difference in the TOF resolutions under different overvoltages is also smaller than 26.3 ± 1.6 ps. The observed TOF resolution between segment 14 and 15 of the T0 counter gradually deteriorates as the beam intensity increases. Nevertheless, the observed TOF resolution between segment 14 and 15 is better than 100.3 ± 3.6 ps during hypernuclear production measurement in the WASA-FRS HypHI experiment, even though segment 14 was irradiated by ${}^6\text{Li}$ beams with the highest intensity in all T0 counter segments of up to approximately 3 MHz. Moreover, the TOF

resolution of the T0 counter is inversely correlated to the beam charge Z, and the observed tendency is similar to the observations reported in Refs. [11,18].

CRediT authorship contribution statement

E. Liu: Writing – review & editing, Writing – original draft, Visualization, Software, Project administration, Methodology, Investigation, Formal analysis, Data curation, Conceptualization. **V. Drozd:** Writing – review & editing, Methodology, Investigation. **H. Ekawa:** Writing – review & editing, Visualization, Software, Methodology, Investigation, Data curation, Conceptualization. **S. Escrig:** Writing – review & editing, Methodology, Investigation. **Y. Gao:** Writing – review & editing, Methodology, Investigation. **Y. He:** Writing – review & editing, Methodology, Investigation. **A. Kasagi:** Writing – review & editing, Methodology, Investigation. **M. Nakagawa:** Writing – review & editing, Software, Methodology, Investigation, Conceptualization. **H. Ong:** Writing – review & editing, Methodology, Investigation. **C. Rappold:** Writing – review & editing, Methodology, Investigation. **R. Sekiya:** Writing – review & editing, Methodology, Investigation. **T.R. Saito:** Writing – review & editing, Writing – original draft, Supervision, Project administration, Methodology, Investigation, Funding acquisition, Conceptualization. **X. Tang:** Writing – review & editing, Supervision, Methodology, Investigation. **Y.K. Tanaka:** Software, Methodology, Investigation, Data curation, Conceptualization, Writing – review & editing, Visualization. **H. Wang:** Writing – review & editing, Methodology, Investigation. **A. Yanai:** Writing – review & editing, Methodology, Investigation. **P. Achenbach:** Writing – review & editing, Methodology, Investigation. **H. Alibrahim Alfaki:** Writing – review & editing, Methodology, Investigation. **F. Amjad:** Writing – review & editing, Methodology, Investigation. **M. Armstrong:** Writing – review & editing, Methodology, Investigation. **K.-H. Behr:** Writing – review & editing, Methodology, Investigation. **J. Benlliure:** Writing – review & editing, Methodology, Investigation. **Z. Brencic:** Writing – review & editing, Methodology, Investigation. **T. Dickel:** Writing – review & editing, Methodology, Investigation. **S. Dubey:** Writing – review & editing, Methodology, Investigation. **M. Feijoo-Fontán:** Writing – review & editing, Methodology, Investigation. **H. Fujioka:** Writing – review & editing, Methodology, Investigation. **H. Geissel:** Writing – review & editing, Methodology, Investigation. **F. Goldenbaum:** Writing – review & editing, Methodology, Investigation. **A. Graña González:** Writing – review & editing, Methodology, Investigation. **E. Haettner:** Writing – review & editing, Methodology, Investigation. **M.N. Harakeh:** Writing – review & editing, Methodology, Investigation. **H. Heggen:** Writing – review & editing, Methodology, Investigation. **C. Hornung:** Writing – review & editing, Methodology, Investigation. **N. Hubbard:** Writing – review & editing, Methodology, Investigation. **K. Itahashi:** Writing – review & editing, Methodology, Investigation. **M. Iwasaki:** Writing – review & editing, Methodology, Investigation. **N. Kalantar-Nayestanaki:** Writing – review & editing, Methodology, Investigation. **M. Kavatsyuk:** Writing – review & editing, Methodology, Investigation. **E. Kazantseva:** Writing – review & editing, Methodology, Investigation. **A. Khreptak:** Writing – review & editing, Methodology, Investigation. **B. Kindler:** Writing – review & editing, Methodology, Investigation. **R. Knoebel:** Writing – review & editing, Methodology, Investigation. **H. Kollmus:** Writing – review & editing, Methodology, Investigation. **D. Kostyleva:** Writing – review & editing, Methodology, Investigation. **S. Kraft-Bermuth:** Writing – review & editing, Methodology, Investigation. **N. Kurz:** Writing – review & editing, Methodology, Investigation. **B. Lommel:** Writing – review & editing, Methodology, Investigation. **S. Minami:** Writing – review & editing, Methodology, Investigation. **D.J. Morrissey:** Writing – review & editing, Methodology, Investigation. **P. Moskal:** Writing – review & editing, Methodology, Investigation. **I. Mukha:** Writing – review & editing, Methodology, Investigation. **A. Muneem:** Writing – review & editing, Methodology, Investigation. **K. Nakazawa:** Writing – review & editing, Methodology,

Investigation. **C. Nociforo:** Writing – review & editing, Methodology, Investigation. **S. Pietri:** Writing – review & editing, Methodology, Investigation. **J. Pochodzalla:** Writing – review & editing, Methodology, Investigation. **S. Purushothaman:** Writing – review & editing, Methodology, Investigation. **E. Rocco:** Writing – review & editing, Methodology, Investigation. **J.L. Rodríguez-Sánchez:** Writing – review & editing, Methodology, Investigation. **P. Roy:** Writing – review & editing, Methodology, Investigation. **R. Ruber:** Writing – review & editing, Methodology, Investigation. **S. Schadmand:** Writing – review & editing, Methodology, Investigation. **C. Scheidenberger:** Writing – review & editing, Methodology, Investigation. **P. Schwarz:** Writing – review & editing, Methodology, Investigation. **V. Serdyuk:** Writing – review & editing, Methodology, Investigation. **M. Skurzok:** Writing – review & editing, Methodology, Investigation. **B. Streicher:** Writing – review & editing, Methodology, Investigation. **K. Suzuki:** Writing – review & editing, Methodology, Investigation. **B. Szczepanzyk:** Writing – review & editing, Methodology, Investigation. **N. Tortorelli:** Writing – review & editing, Methodology, Investigation. **M. Vencelj:** Writing – review & editing, Methodology, Investigation. **T. Weber:** Writing – review & editing, Methodology, Investigation. **H. Weick:** Writing – review & editing, Methodology, Investigation. **M. Will:** Writing – review & editing, Methodology, Investigation. **K. Wimmer:** Writing – review & editing, Methodology, Investigation. **A. Yamamoto:** Writing – review & editing, Methodology, Investigation. **J. Yoshida:** Writing – review & editing, Methodology, Investigation. **J. Zhao:** Writing – review & editing, Methodology, Investigation.

Declaration of competing interest

The authors declare that they have no known competing financial interests or personal relationships that could have appeared to influence the work reported in this paper.

Data availability

Data will be made available on request.

Acknowledgments

The two WASA-FRS experiments, S447 and S490 were performed in 2022 at the FRS at the GSI Helmholtzzentrum fuer Schwerionenforschung, Darmstadt (Germany) in the context of FAIR Phase 0. The authors would like to acknowledge the GSI staff for their supports in the experiment. The WASA-FRS project is supported by the JSPS KAKENHI, Japan (Grant Numbers JP18H01242), the JSPS Grant-in-Aid for Early-Career Scientists (Grant No. JP20K14499), the JSPS Fostering Joint International Research (B) (Grant No. JP20KK0070), Proyectos I+D+i 2020 ref: PID2020-118009GA-I00 ; grant 2019- T1/TIC-13194 of the program Atracción de Talento Investigador of the Community of Madrid, the Regional Government of Galicia under the Postdoctoral Fellowship Grant No. ED481D-2021-018, the “Ramón y Cajal” program under the Grant No. RYC2021-031989-I, the SciMat and qLife Priority Research Areas budget under the program Excellence Initiative - Research University at the Jagiellonian University and the European Unions Horizon 2020 research and innovation programme under grant agreement No 824093. The project is also supported by the Justus-Liebig-Universität (JLU), Gießen, Germany, and GSI, Germany under the JLU-GSI strategic Helmholtz partnership agreement. This research is supported in part by the ExtreMe Matter Institute EMMI at the GSI Helmholtzzentrum fuer Schwerionenforschung, Darmstadt, Germany. The authors thank Luise Doersching-Steitz of GSI, Rita Krause of GSI, Yukiko Kurakata of RIKEN, Daniela Press of GSI, Miao Yang of IMP and Xiaohua Yuan of IMP for supporting the projects, including the administrative works.

References

- [1] A. Gal, E.V. Hungerford, D.J. Millener, Strangeness in nuclear physics, *Rev. Modern Phys.* 88 (3) (2016) <http://dx.doi.org/10.1103/revmodphys.88.035004>.
- [2] H. Lenske, Theory and applications of nuclear direct reactions, *Internat. J. Modern Phys. E* 30 (10) (2021) 2130010.
- [3] T.R. Saito, et al., New directions in hypernuclear physics, *Nat. Rev. Phys.* (2021) <http://dx.doi.org/10.1038/s42254-021-00371-w>.
- [4] T.R. Saito, Studies of hypernuclei with heavy-ion beams, nuclear emulsions and machine learning, *EPJ Web Conf.* 271 (2022) 08003, <http://dx.doi.org/10.1051/epjconf/202227108003>.
- [5] H. Ekawa, WASA-FRS HypHI experiment at GSI for studying light hypernuclei, *EPJ Web Conf.* 271 (2022) 08012, <http://dx.doi.org/10.1051/epjconf/202227108012>.
- [6] C. Rappold, T.R. Saito, Hypernuclear spectroscopy with heavy-ion beams: Present status and perspectives, in: N.A. Orr, M. Płoszajczak, F.M. Marqués, J. Carbonell (Eds.), *Recent Progress in Few-Body Physics*, Springer International Publishing, Cham, 2020, pp. 913–921.
- [7] T. Saito, P. Achenbach, H.A. Alfaki, F. Amjad, M. Armstrong, K.-H. Behr, J. Benlliure, Z. Brencic, T. Dickel, V. Drozd, S. Dubey, H. Ekawa, S. Escrig, M. Feijoo-Fontán, H. Fujioka, Y. Gao, H. Geissel, F. Goldenbaum, A.G. González, E. Haettner, M. Harakeh, Y. He, H. Heggen, C. Hornung, N. Hubbard, K. Itahashi, M. Iwasaki, N. Kalantar-Nayestanaki, A. Kasagi, M. Kavatsyuk, E. Kazantseva, A. Khreptak, B. Kindler, R. Knoebel, H. Kollmus, D. Kostyleva, S. Kraft-Bermuth, N. Kurz, E. Liu, B. Lommel, V. Metag, S. Minami, D. Morrissey, P. Moskal, I. Mukha, A. Muneem, M. Nakagawa, K. Nakazawa, C. Nociforo, H. Ong, S. Pietri, J. Pochodzalla, S. Purushothaman, C. Rappold, E. Rocco, J. Rodríguez-Sánchez, P. Roy, R. Ruber, S. Schadmand, C. Scheidenberger, P. Schwarz, R. Sekiya, V. Serdyuk, M. Skurzok, B. Streicher, K. Suzuki, B. Szczepanczyk, Y. Tanaka, X. Tang, N. Tortorelli, M. Vencelj, H. Wang, T. Weber, H. Weick, M. Will, K. Wimmer, A. Yamamoto, A. Yanai, J. Yoshida, J. Zhao, The WASA-FRS project at GSI and its perspective, *Nucl. Instrum. Methods Phys. Res. B* 542 (2023) 22–25, <http://dx.doi.org/10.1016/j.nimb.2023.05.042>.
- [8] H. Geissel, P. Armbruster, K. Behr, A. Brünle, K. Burkard, M. Chen, H. Folger, B. Franczak, H. Keller, O. Klepper, B. Langenbeck, F. Nickel, E. Pfeng, M. Pfützner, E. Roeckl, K. Rykaczewski, I. Schall, D. Schardt, C. Scheidenberger, K.-H. Schmidt, A. Schröter, T. Schwab, K. Sümmerer, M. Weber, G. Münzenberg, T. Brohm, H.-G. Clerc, M. Fauerbach, J.-J. Gaimard, A. Grewe, E. Hanelt, B. Knödler, M. Steiner, B. Voss, J. Weckenmann, C. Ziegler, A. Magel, H. Wollnik, J. Dufour, Y. Fujita, D. Vieira, H. Sherrill, The GSI projectile fragment separator (FRS): a versatile magnetic system for relativistic heavy ions, *Nucl. Instrum. Methods Phys. Res. B* 70 (1) (1992) 286–297, [http://dx.doi.org/10.1016/0168-583X\(92\)95944-M](http://dx.doi.org/10.1016/0168-583X(92)95944-M), URL <https://www.sciencedirect.com/science/article/pii/0168583X9295944M>.
- [9] C. Bargholtz, M. Bashkanov, M. Berłowski, A. Bondar, D. Bogoslawsky, W. Brodowski, J. Brudvik, H. Calén, F. Capellaro, A. Chilingarov, H. Clement, J. Comfort, L. Demirörs, C. Ekström, K. Fransson, C.-J. Fridén, L. Gerén, M. Gornov, V. Grebenov, J. Greiff, Y. Gurov, L. Gustafsson, B. Høistad, G. Ivanov, M. Jacewicz, E. Jiganov, A. Johansson, T. Johansson, S. Keleta, O. Khakimova, A. Khoukaz, K. Kilian, N. Kimura, I. Koch, G. Kolachev, F. Kren, S. Kullander, A. Kupś, A. Kuzmin, A. Kuznetsov, K. Lindberg, P. Marciniewski, R. Meier, O. Messner, B. Morosov, A. Nawrot, B. Nefkens, G. Norman, W. Oelert, C. Pauly, H. Pettersson, A. Pivovarov, J. Pätzold, Y. Petukhov, A. Povtorejko, D. Reistad, R. Ruber, S. Sandukovskiy, K. Schönning, W. Scobel, T. Seifzick, R. Shafiqullin, B. Shwartz, V. Sidorov, T. Skorodko, V. Sopov, A. Starostin, J. Stepaniak, A. Sukhanov, A. Sukhanov, V. Tchernyshev, P.-E. Tegnér, P.T. Engblom, V. Tikhomirov, H. Toki, A. Turowiecki, G. Wagner, U. Wiedner, Z. Wilhelmi, M. Wolke, A. Yamamoto, H. Yamaoka, J. Zabierowski, I. Zartova, J. Złomańczuk, The WASA detector facility at CELSIUS, *Nucl. Instrum. Methods Phys. Res. A* 594 (3) (2008) 339–350, <http://dx.doi.org/10.1016/j.nima.2008.06.011>.
- [10] C. Höppner, S. Neubert, B. Ketzer, S. Paul, A novel generic framework for track fitting in complex detector systems, *Nucl. Instrum. Methods Phys. Res. A* 620 (2–3) (2010) 518–525, <http://dx.doi.org/10.1016/j.nima.2010.03.136>.
- [11] R. Sekiya, V. Drozd, Y. Tanaka, K. Itahashi, H. Fujioka, S. Matsumoto, T. Saito, K. Suzuki, Time resolution and high-counting rate performance of plastic scintillation counter with multiple MPPC readout, *Nucl. Instrum. Methods Phys. Res. A* 1034 (2022) 166745, <http://dx.doi.org/10.1016/j.nima.2022.166745>, URL <https://www.sciencedirect.com/science/article/pii/S0168900222002650>.
- [12] J. Kataoka, A. Kishimoto, T. Fujita, T. Nishiyama, Y. Kurei, T. Tsujikawa, T. Oshima, T. Taya, Y. Iwamoto, H. Ogata, H. Okochi, S. Ohsuka, H. Ikeda, S. Yamamoto, Recent progress of MPPC-based scintillation detectors in high precision X-ray and gamma-ray imaging, *Nucl. Instrum. Methods Phys. Res. A* 784 (2015) 248–254, <http://dx.doi.org/10.1016/j.nima.2014.11.004>, URL <https://www.sciencedirect.com/science/article/pii/S0168900214012522>, Symposium on Radiation Measurements and Applications 2014 (SORMA XV).
- [13] R. Onda, K. Ieki, T. Iwamoto, S. Kobayashi, N. Matsuzawa, T. Mori, M. Nakao, M. Nishimura, S. Ogawa, W. Ootani, Y. Uchiyama, Optimal design of plastic scintillator counter with multiple sipm readouts for best time resolution, *Nucl. Instrum. Methods Phys. Res. A* 936 (2019) 563–564, <http://dx.doi.org/10.1016/j.nima.2018.10.070>, URL <https://www.sciencedirect.com/science/article/pii/S0168900218313846>, Frontier Detectors for Frontier Physics: 14th Pisa Meeting on Advanced Detectors.
- [14] M. Bazzi, C. Berucci, G. Corradi, C. Curceanu, A. D’Uffizi, K. Piscicchia, M. Poli Lener, A. Rizzo, A. Romero Vidal, E. Sbardella, A. Scordo, D. Tagnani, O. Vazquez Doce, Experimental tests of the trigger prototype for the AMADEUS experiment based on Sci-Fi read by MPPC, *Nucl. Instrum. Methods Phys. Res. A* 671 (2012) 125–128, <http://dx.doi.org/10.1016/j.nima.2011.12.102>, URL <https://www.sciencedirect.com/science/article/pii/S0168900211023552>.
- [15] M. Nishimura, F. Berg, M. Biasotti, G. Boca, P. Cattaneo, M. De Gerone, A. De Bari, M. Francesconi, L. Galli, F. Gatti, U. Hartmann, Z. Hodge, P.-R. Kettle, M. Nakao, D. Nicol, W. Ootani, A. Papa, S. Ritt, M. Rossella, E. Schmid, Y. Uchiyama, M. Usami, K. Yanai, Full system of positron timing counter in MEG II having time resolution below 40 ps with fast plastic scintillator readout by SiPMs, *Nucl. Instrum. Methods Phys. Res. A* 958 (2020) 162785, <http://dx.doi.org/10.1016/j.nima.2019.162785>, URL <https://www.sciencedirect.com/science/article/pii/S0168900219312318>, Proceedings of the Vienna Conference on Instrumentation 2019.
- [16] M. Cortés, M. Reese, S. Doublet, S. Saha, H. Schaffner, F. Ameil, P. Bednarczyk, J. Gerl, M. Gorska, N. Pietralla, J. Vesic, Silicon photomultipliers as readout for a segmented time-of-flight plastic detector, *Nucl. Instrum. Methods Phys. Res. A* 899 (2018) 101–105, <http://dx.doi.org/10.1016/j.nima.2018.05.031>, URL <https://www.sciencedirect.com/science/article/pii/S0168900218306363>.
- [17] A. Stoykov, T. Rostomyan, Time resolution of BC422 plastic scintillator read out by a SiPM, *IEEE Trans. Nucl. Sci.* 68 (7) (2021) 1487–1494, <http://dx.doi.org/10.1109/TNS.2021.3089616>.
- [18] P.W. Cattaneo, M. De Gerone, F. Gatti, M. Nishimura, W. Ootani, M. Rossella, Y. Uchiyama, Development of high precision timing counter based on plastic scintillator with SiPM readout, *IEEE Trans. Nucl. Sci.* 61 (5) (2014) 2657–2666, <http://dx.doi.org/10.1109/TNS.2014.2347576>.
- [19] P. Achenbach, C.A. Gayoso, J. Bernauer, R. Böhm, M. Distler, L. Doria, J. Friedrich, H. Merkel, U. Müller, L. Nungesser, J. Pochodzalla, S.S. Majos, S. Schlimme, T. Walcher, M. Weinriefer, Measurement of propagation time dispersion in a scintillator, *Nucl. Instrum. Methods Phys. Res. A* 578 (1) (2007) 253–260, <http://dx.doi.org/10.1016/j.nima.2007.05.210>.
- [20] Hamamatsu Photonics, MPPC S13615 series, 2021, URL https://www.hamamatsu.com/content/dam/hamamatsu-photonics/sites/documents/99_SALES_LIBRARY/ssd/s13615_series_kapd1062e.pdf. (Accessed 15 June 2023).
- [21] Kikusui Electronics Corp., User’s manual for regulated DC power supply, PMX series 2023, URL https://kikusui-korea.co.kr/files/PDF/PMX_A_M.pdf. (Accessed 16 November 2023).
- [22] R. Ruber, Doctoral dissertation, Uppsala University, 1999.
- [23] R. Ruber, M. Blom, H. Calén, C.-J. Fridén, A. Larsson, G. Norman, A. Yamamoto, H. Yamaoka, Y. Makida, N. Kimura, K. Tanaka, M. Iida, H. Ohhata, H. Hirabayashi, N. Takasu, A. Nawrot, An ultra-thin-walled solenoid for the CELSIUS/WASA experiments, *Nucl. Instrum. Methods Phys. Res. A* 503 (3) (2003) 431–444, [http://dx.doi.org/10.1016/S0168-9002\(03\)00995-1](http://dx.doi.org/10.1016/S0168-9002(03)00995-1).
- [24] B. Jurado, K.-H. Schmidt, K.-H. Behr, Application of a secondary-electron transmission monitor for high-precision intensity measurements of relativistic heavy-ion beams, *Nucl. Instrum. Methods Phys. Res. A* 483 (3) (2002) 603–610, [http://dx.doi.org/10.1016/S0168-9002\(01\)01931-3](http://dx.doi.org/10.1016/S0168-9002(01)01931-3).
- [25] mesytec GmbH & Co. K.G., MCFD-16, 2021, URL <https://www.mesytec.com/products/datasheets/MCFD-16.pdf>. (Accessed: 30 March 2023).
- [26] W. Ootani, K. Ieki, T. Iwamoto, D. Kaneko, T. Mori, S. Nakaura, M. Nishimura, S. Ogawa, R. Sawada, N. Shibata, Y. Uchiyama, K. Yoshida, K. Sato, R. Yamada, Development of deep-UV sensitive MPPC for liquid xenon scintillation detector, *Nucl. Instrum. Methods Phys. Res. A* 787 (2015) 220–223, <http://dx.doi.org/10.1016/j.nima.2014.12.007>.
- [27] Hamamatsu Photonics, Handbook of Si APD and MPPC, 2021, URL http://laser-mediaservices.de/download/1121_1_4_1679_4_1_178/hamamatsuphotonics_handbook_si_apd_mppc.pdf. (Accessed: 14 December 2023).
- [28] A. Ulyanov, D. Murphy, J. Mangan, V. Gupta, W. Hajdas, D. de Faoite, B. Shortt, L. Hanlon, S. McBreen, Radiation damage study of sensL J-series silicon photomultipliers using 101.4 MeV protons, *Nucl. Instrum. Methods Phys. Res. A* 976 (2020) 164203, <http://dx.doi.org/10.1016/j.nima.2020.164203>.